Progress In Electromagnetics Research B, Vol. 93, 47–65, 2021

Salt Water Exposure Effects on Single-Layer, Unidirectional Carbon-Fiber Reinforced Polymer Circuit Analog Absorbers

Joseph C. O'Donnell[1, 2] and Ram M. Narayanan[1, 2, *]

Abstract—This paper explores the effects of extended exposure to salt water fog on the microwave absorption properties of unidirectional carbon-fiber reinforced polymer (CFRP) circuit analog absorbers (CAA). Single-layer CFRP CAAs were fabricated using a wet-layup technique and were then subjected to a controlled salt water fog chamber following B117 standards. A total of ten samples using 305 g/m^2 areal-weight unidirectional CFRP were fabricated. Three samples were withdrawn from the salt water environment at ten-day intervals and tested, with the final samples being withdrawn after 30 days. The mass of each sample was measured immediately after removal to measure mass-accumulation and after a five-day interval to measure mass-loss. A free space microwave reflection measurement system was implemented to track and quantify changes to the absorption capabilities of the CAA. A physically-based electromagnetic model was developed to characterize the changes caused by salt water absorption, and good agreement was observed with measured data.

1. INTRODUCTION

The use of fiber composites in sea and air craft is becoming increasingly popular, primarily due to their beneficial mechanical and structural properties [1, 2]. Composites are used in subsystems, individual structures, and complete crafts. Carbon-fiber reinforced-polymers (CFRPs) in particular offer favorable properties such as high directional strength, low weight, and fatigue and corrosion resistance. Carbon-fiber composites do have some inherent weaknesses, however, in that they are vulnerable to external impact damages as well as moisture penetration and absorption [1]. Epoxy resin, commonly used as a curing agent in composites, is also susceptible to moisture absorption. The mechanical and structural effects that composites experience under salt water and moisture exposure are well documented [3–5]. Carbon-epoxy composites in particular are vulnerable to swelling, buckling, and rippling due to moisture absorption, which in turn significantly reduces their mechanical properties [6, 7]. More physical and structural changes caused by moisture or brine absorption, and how those changes relate to this work, are discussed in the next section.

The focus of this paper, the electromagnetic effects experienced by composite absorbers when exposed to salt water fog, is notably less documented in the open literature. Some papers discuss change to the dielectric properties of composite materials in isolation, such as CFRP and graphite fiber reinforced polymers (GFRP) [8, 9]. While documentation on moisture's effect on radar absorbing materials (RAM) is available in the open literature, to the authors' knowledge, no research has been published on the electromagnetic effects of salt water on composites used in radar absorbing materials (RAMs). These structural changes could alter the electromagnetic properties of the CFRP as well. As moisture penetrates the composite layer, the dielectric properties of the structure are expected to change. For CFRPs in use in sandwich-structure RAMs, the absorption profile of the absorber could also

Received 22 May 2021, Accepted 20 July 2021, Scheduled 24 July 2021
* Corresponding author: Ram M. Narayanan (rmn12@psu.edu).
[1] Department of Electrical Engineering, Pennsylvania State University, University Park, PA 16802, USA. [2] Applied Research Laboratory, University Park, PA 16802, USA.

change significantly. The operation of CAAs and the classical Salisbury screens are discussed in [10, 11]. It is evident from [10, 11] that successful absorption depends on the physical structure of the absorber and the electromagnetic properties of its components. The components of a sandwich structure, like the ones studied in this paper, include the spacer material and the composite material. Any change the geometry of the absorber will affect the electromagnetics of the absorber. Thus, it is desired that the geometry and electromagnetic properties of its components do not change throughout the service life of the absorber. The CFRP CAAs studied in this paper often operate in salt water rich environments and, as a result, are vulnerable to physical and electromagnetic changes due to salt water moisture. Any significant change to the physical and electromagnetic properties of the absorber would require either repair or replacement to avoid detrimental performance during service.

Previous work by the authors showed how impact damage causes unique changes in the physical structure, and thus the electromagnetic characteristics, of the CFRP sandwich structure [12]. A simple full-wave electromagnetic model was created in which the complex and random nature of impact damage could be straightforwardly represented and changes to the absorption profile of the absorber could be tracked.

This paper explores the effects of extended exposure to salt water fog on CFRP circuit-analog absorbers. CAAs in this work take the form of CFRP-foam-aluminum sandwich structures and are designed to absorb incident energy at X-band frequencies (between 8 and 12.4 GHz). Following fabrication techniques presented and discussed in [13–15], ten, single-ply, unidirectional CFRP CAAs were fabricated using $305\,\mathrm{g/m^2}$ areal-weight CFRP. The ten absorbers were introduced inside the salt water fog chamber simultaneously. At intervals of ten days (14400 minutes), three samples were randomly removed from the salt water chamber for microwave reflectivity measurements. The final removal pulled four samples that were each exposed for a total of thirty days (43200 minutes). Metrics such as mass, pH, pressure, temperature, and fall-out were recorded throughout the experimentation. The electromagnetic properties of the "before-and-after exposure" samples were measured using a vector network analyzer (VNA) and compared to understand the effect of salt water on the absorption profile of the absorbers.

The primary objective of this study is to quantify deterioration in the absorption profile of CFRP CAAs due to salt water exposure, build a simple full-wave electromagnetic model that adheres to known and witnessed physical changes, and compare these model results to measured results. Any assumptions that are taken in the development of this full-wave model are expressed explicitly.

The organization of this paper is as follows. Section 2 reviews physical and structural changes commonly experienced by composite surfaces during moisture or salt water exposure. Section 2 also discusses the salt water exposure methodology. Section 3 presents some sample electromagnetic simulations based on some potential physical changes discussed in Section 2. Section 3 also discusses the electromagnetic measurement interface, material characterization terminology, and sample fabrication. Section 4 presents the results of extended salt water corrosion on CFRP CAAs and compares the experimental and modeled results. Conclusions are presented in Section 5.

2. POTENTIAL EFFECTS FROM SALT WATER EXPOSURE

Extensive investigations in the open literature have established that moisture and salt water exposure affect the physical and structural properties of fiber-matrix composites. Matrix cracking, delaminations, debonding, and swelling all often occur due to moisture and salt water exposure. Mechanical properties of epoxy matrices such as tensile strength, compression strength, residual strength, shear strength, impact resistance, and elongation are shown to deteriorate significantly as the moisture content in the composite increases [6]. The composite's fiber architecture (unidirectional, woven, twill-weave, etc.) affects the severity of mechanical property degradation as a result of moisture exposure [7]. Fiber-epoxy composites are shown to continue to absorb moisture for over 40 days in [7, 16] and over 80 hours in [17]. Salt-crystal formation is shown to occur on CFRP surfaces when exposed to salt water in [18].

There have been limited investigations of moisture and salt water exposure effects on the electromagnetic properties of composites, however. Water immersion time is shown to directly affect the conductivity and complex relative permittivity in carbon fiber-epoxy composites [8] and graphite fiber-epoxy composites [9]. Further electromagnetic properties changes due to moisture contamination are

shown in [19–21]. Moisture is observed to affect the relative permittivity of composites in radomes [19]. Following this discussion and experience from prior work of the authors, unidirectional CFRP CAAs seem to be susceptible to structural changes when exposed to a salt water environment. Salt-crystal formations on the CFRP surface may alter the complex sheet impedance of the CFRP sheet. Potential moisture penetration through the CFRP-epoxy matrix can severely alter the dielectric properties of the dielectric spacer and cause swelling as the epoxy matrix or spacer absorbs moisture. Swelling in sandwich-structure absorbers, in both the surface layer and the spacer layer would significantly alter the absorption performance of the absorber as the thickness of the layers increase. Furthermore, rippling in the CFRP-epoxy matrix may occur as the matrix absorbs moisture and weakens. Rippling on the surface may also contribute to an increase in the effective thickness of the surface layer.

2.1. Moisture Exposure Methodology

In this work, ten CAA samples are placed within a salt water fog chamber and are held upright at a slightly backward slant by plastic channels. The samples are spaced such that the fog can easily access each of the samples and condensed moisture dripping off of one sample cannot contact another sample. The samples are positioned towards the side of the chamber and are facing forwards. The samples are not touched again until they are removed from the chamber. The orientation and spacing of the samples ensures that the removal of a sample will not affect other samples' exposure to salt water.

The salt water chamber used is a Singleton Cyclic Corrosion Test (CCT) chamber. The salt water exposure methodology used here follows closely that of ASTM G85. The salt water solution is 3.5% salt. At 24-hour intervals, instrumentation values are recorded and measurements are made. The chamber temperature, the tower temperature, and the tower air pressure are recorded while the cycle is running. The cycle is then paused and the chamber is purged of salt fog. The purge cycle is allowed to run for about 15 minutes before the chamber is opened. Near and far fallout within the chamber are measured, as well as salt water solution pH and specific gravity. The pH of the fallout is measured using a ThermoFisher Scientific Orion 8165BNWP ROSS Sure-Flow pH Electrode. The electrode was carefully rinsed off with distilled water before and after pH measurements and then promptly returned to the proper storage solution. More salt water solution is added to the reservoir as needed. The chamber is closed and the cycle is continued.

The samples are brought directly to the free space microwave reflection measurement system after they are pulled from the salt water chamber. A maximum delay of thirty minutes occurs between removal from the chamber and reflectivity measurements. The mass accumulation for each sample is recorded at this time as well to get a measure of the moisture absorption and absorber saturation. There was noticeable moisture accumulation on each of the samples, and the samples were disturbed as little as possible prior to reflectivity measurements. Note that during measurements some of the accumulated moisture collected into drops and fell off the sample due to gravity. Sample mass is

Figure 1. Rippling and salt crystal formation due to a fiber-matrix weakening seen after salt water exposure and removed from the chamber after five days.

Table 1. Salt water exposure test parameter values. Bold dates signify that samples were pulled on that date.

Date (MM/DD)	Time	Chamber Temp (F)	Tower Temp (F)	Tower Air Pressure (psi)	Fallout (mL/hr) (near/far)	pH	Specific Gravity
11/19	15:31	95	118	16.0	1.20/1.30	6.63	
11/20	14:01	95	118	15.8	1.13/1.29	6.63	1.035
11/21	14:00	95	118	15.9	1.29/1.38	6.66	
11/22	14:01	95	118	16.1	1.29/1.13	6.69	1.035
11/25	14:03	96	118	16.1	1.19/1.32	6.68	1.035
11/26	14:05	96	118	16.0	1.21/1.38	6.69	
11/27	14:10	95	119	16.0	1.08/1.29	6.59	1.035
12/02	14:00	95	118	15.9	1.25/1.35	6.61	1.035
12/03	14:10	95	118	16.0	1.25/1.33	6.35	
12/04	14:05	95	118	16.0	1.17/1.21	6.40	1.035
12/05	14:00	96	118	16.1	1.25/1.25	6.24	
12/06	14:00	96	118	15.9	1.00/1.13	6.20	1.035
12/09	14:05	95	118	16.0	1.13/1.19	6.68	1.034
12/10	14:01	95	118	16.0	0.88/1.29	6.66	
12/11	14:05	95	118	15.7	1.38/1.08	6.60	1.035
12/12	14:05	95	118	16.0	1.08/1.29	6.52	
12/13	14:05	95	118	15.9	1.17/1.04	6.42	1.035
12/16	16:10	95	119	16.1	1.20/1.11	6.76	1.035
12/17	14:35	95	118	15.9	0.95/1.55	7.12	
12/18	14:10	98	119	16.2	1.21/0.96	6.66	1.035

recorded again after five days to measure mass loss. Recorded instrumentation values and measurements are displayed in Table 1. Note that no measurements were taken during the weekends due to laboratory access limitations. As a result, data were only recorded on 20 days out of the 30-day period. Most instrumentation values and measurements were stable throughout the experimentation process. There is some small variance in the near/far fallout, but all of the values fall within the expected range. Photographs showing a sample five days after being pulled from the chamber are provided in Fig. 1. Rippling in the CFRP layer, which is indicative of a weakening of the fiber-epoxy matrix, and salt crystal formation is evident in Fig. 1. Even though these photographs were taken five days after the respective sample were pulled from the chamber, rippling and swelling were observed immediately after pull. Rippling in each sample is attributed to matrix weakening, or weakening in the epoxy, and debonding. Swelling is attributed to salt water penetrating the CFRP-epoxy layer and the foam layer and also due to the surface tension of the water.

3. MATERIALS AND METHODS

3.1. Experimentation Methods

The free space measurement system used in this work is composed of a pair of radio frequency (RF) probes, a vector network analyzer (VNA), and a control computer. The measurement system captures scattering parameter data for a planar sample located between the RF probes. An acrylic frame holds the sample in place and also aids in angular alignment for measurements. Calibration of the measurement system involves the use of a 0.1-ns time gate for S_{11} reflection coefficient measurements to

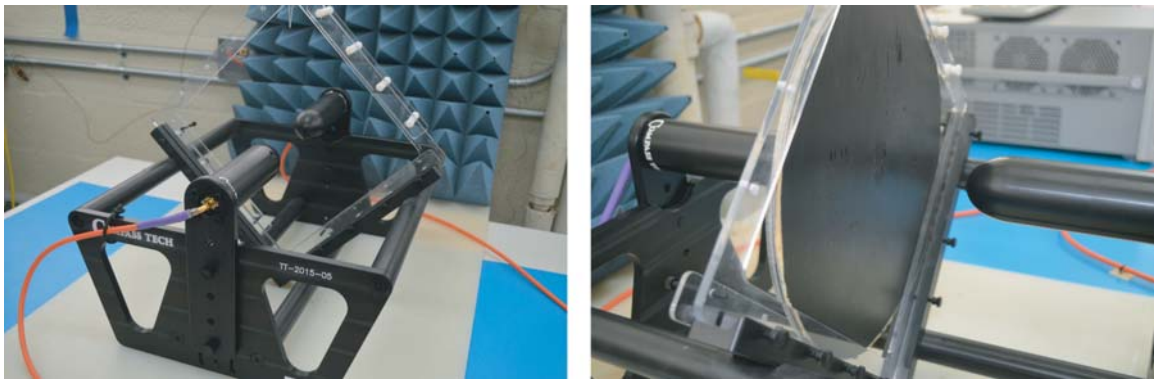

(a) (b)

Figure 2. The free space measurement system. (a) Empty fixture. (b) Inserted sample.

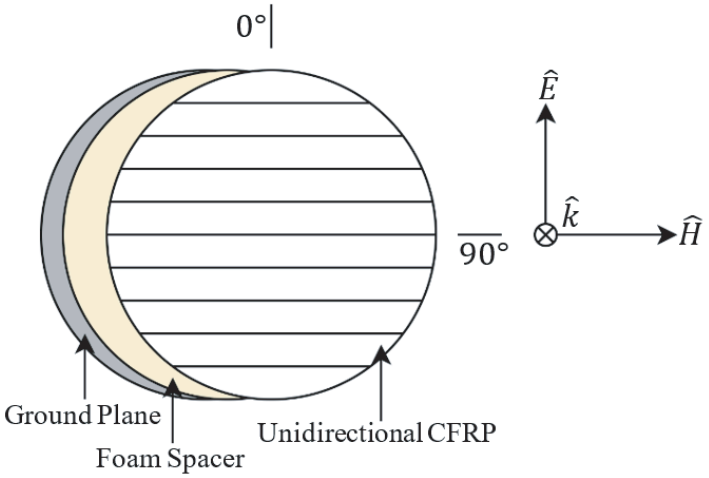

Figure 3. Sample and electromagnetic wave geometry.

reduce multipath effects. The measurement system also requires open and short circuit calibrations for S_{11} measurements for background noise and reference phase information, respectively. Open circuit calibrations can be achieved by measuring free space between the two RF probes. Short circuit calibrations can be achieved by measuring the reflection of a highly-reflective metal plate, which in this work was an aluminum plate. The position of the front face of the aluminum plate determines the reference phase position during sample measurements. Fig. 2 shows the free space measurement system with and without the sample inserted. Angle designations and electromagnetic wave geometry are also presented in Fig. 3. VNA settings used throughout this work are shown in Table 2.

Table 2. Vector Network Analyzer settings.

Points	Frequency Range (GHz)	Power (dBm)
10001	4–18	−5

Ten samples are fabricated in total. Each sample is a CFRP-foam-aluminum sandwich structure. In this work, the unidirectional CFRP used is a 305 g/m^2 areal-weight, standard modulus fabric. The dielectric foam spacer is a 3 lb. density, closed cell vinyl foam. Its dielectric constant is nominally 1.05 [22]. No data could be found regarding moisture absorption or thickness increases for the foam

used. The aluminum is a 1.27 mm thick, cold rolled, hardened, 6061 aluminum sheet. The CFRP, foam, and aluminum were all cut into 304.8 mm diameter circles. Epoxy resin was mixed by hand and then applied to the CFRP sheets. The foam cores were placed on top of the CFRP sheets and gentle pressure was applied evenly across the surface to aid in curing. After the CFRP-foam samples were fully cured under atmospheric pressure and room temperature, the CFRP-foam and aluminum sheets were cured together using the same technique. It is assumed that a small amount of epoxy bled into the foam from both sides during curing. It is also assumed that the bleeding has a negligible effect on the electromagnetics of the structure. Finally, a layer of epoxy and liquid rubber was applied to seal the edges of the surface such that moisture penetration is only possible through the composite material. At each step in the curing process, the mass of each sample was recorded and is shown in Table 3. The presence of voids in the front surface of some of the samples was noted.

Table 3. The dry and cured weights of each sample.

Sample	A	B	C	D	E	F	G	H	I	J
Dry Mass (g)										
CFRP	23.10	22.96	23.10	23.10	23.70	23.50	23.80	23.80	23.50	23.70
Foam	10.77	10.49	10.76	10.88	10.80	10.70	10.90	10.60	9.80	12.70
Aluminum	246.78	248.34	249.33	248.06	247.30	247.50	249.30	249.30	247.50	248.00
Total	280.65	281.79	283.19	281.94	281.80	281.7	284.00	283.60	280.80	284.40
Cured Mass (g)										
Total pre-seal	334.2	304.2	309.1	329.5	320.9	315.8	311.0	316.6	312.6	317.8
Total post-seal	355.8	326.9	331.7	349.3	346.9	343.6	334.3	339.3	337.7	337.9
Mass after pull (g)										
Total 30 min post	361.8	333.6	339.7	362.2	359.8	353.1	347.3	347.2	348.7	345.3
Total 5 days post	356.8	327.7	332.5	351.7	351.3	345.6	343.5	342.5	344.1	341.0

After curing, each sample is marked in 15 degree intervals from 0° to 90° in relation to the fiber direction. 0° corresponds with parallel to the fiber direction, while 90° corresponds with perpendicular to the fiber direction. Reflectivity data were captured at each marking for each sample using the free space measurement interface described in Section 3. Reflectivity data were captured after curing to gather initial state data, and were captured after salt water exposure for comparison. After initial state reflectivity data are captured, the samples are ready for salt water exposure.

Furthermore, relative permittivity data for each sample were measured before and after salt water exposure in the free space measurement system. Before the aluminum sheets were cured to the CFRP-foam samples, the CFRP-foam samples were placed in the free space measurement system, and S_{21} data were collected. Then, an algorithm was implemented to extract the complex permittivity data of each sample from the S_{21} data. S_{11} data were then captured after the aluminum sheets were cured to the CFRP-foam samples. As mentioned in [12], each sample is fundamentally different largely due to inherent variability in CFRP fabric and the wet-layup fabrication method. Thus, the complex permittivities of the samples are also different from one another. The complex permittivities of the samples were measured again after salt water exposure after the aluminum sheet was removed from the sample.

3.2. Electromagnetic Simulations

This section presents simulations detailing some possible effects of moisture contamination on the reflection coefficient of an exemplar resonant electromagnetic absorber based on the preceding discussions. To estimate the amount of moisture that penetrates into the absorber, the CFRP CAA is modeled in three distinct ways. The first model represents the CFRP layer as an infinitely thin resistive sheet. The second model represents the CFRP layer as a 0.28-mm thick, anisotropic, complex-impedance dielectric sheet. Moisture contamination is handled similarly in both models. Again, these two models are used to estimate the amount of moisture that penetrates into the foam layer. As such, the thickness of the CFRP layer remains constant for each respective model. The final model represents a two-variable model in which moisture absorption occurs in both the foam layer and CFRP layer. The final model differs from the previous two in that the CFRP layer is allowed to vary in thickness. Differences between the three models are summarized in Table 4.

Table 4. Differences among the three full-wave models presented in this paper.

Model	Purpose	Assumptions
Infinitely Thin Resistive Sheet	To analyze salt water absorption in a sample Salisbury screen absorber	• CFRP layer is infinitely thin and its surface impedance is purely real • CFRP layer is not affected by brine • Foam layer forms effective medium with brine
Finite Thickness Impedance Sheet	To estimate the amount of brine that could penetrate the foam layer	• CFRP layer is of 0.28-mm thickness and its surface impedance is complex • CFRP layer is not affected by brine • Foam layer forms effective medium with brine
Two-Variable Model	To realistically model brine contamination in the CFRP CAA	• CFRP layer and foam layer are both affected by brine • CFRP thickness increases due to brine contamination • Foam layer forms effective medium with brine

These full-wave models are similar to the full-wave model introduced for impact damage [12]. Salt water exposure affects CFRP differently than impact damage as discussed in the section above and in [12], however. Thus the full-wave model will also have differences. Throughout this paper, the full-wave model for salt water exposure will be completely explained and the differences between the salt water exposure and impact damage will be explored after results are presented.

The first two models will be discussed first. These simulations depict the results of saline moisture penetrating through the CFRP sheet completely and contaminating the foam spacer. The assumption in these models is that moisture absorption occurs only in the foam layer. It is also assumed in these models that the thickness of the CFRP layer remains constant, regardless of amount of absorption. Under these conditions, the contaminating moisture and foam spacer will form an effective medium with a new effective relative permittivity. Effective medium theory is well documented in [19], but that is outside the scope of this work. These example simulations show the potential effect of increasing the volume fraction of saline moisture to foam on the absorption profile of the CAA. The following method is used to create the full-wave simulation models in FEKO.

The free space model creation is documented in Fig. 4. The first surface constructed is the PEC ground plane centered at the origin. A cuboid, which represents the foam spacer material, is then constructed and positioned above the ground plane. The thickness of the cuboid is set equal to the measured thickness of the foam spacer, h, and is initially given a frequency-independent relative permittivity of 1.05. It is assumed in the model that the relative permittivity of the foam spacer will not remain constant and is instead a function of saline moisture contamination. The relative permittivity of the new effective medium is of the form $\varepsilon_{\text{eff}} = \varepsilon_0\varepsilon_r(1 - j\tan\delta)$, where ε_0 is the relative permittivity of free space and tan δ is the loss tangent. The last surface constructed is a flat rectangle that represents

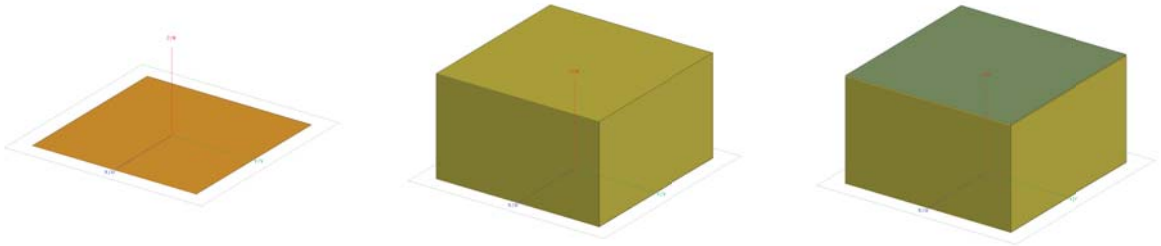

(a) (b) (c)

Figure 4. (a) PEC square located at $z = 0$. (b) Foam layer added to the model as a cuboid. (c) Unidirectional CFRP added to the model as a square with anisotropic properties.

the CFRP sheet and is positioned immediately above the cuboid. In the model, the thickness of the layer is captured in the dielectric properties of the surface. Thus, this flat rectangle will remain flat and its thickness does not need to be defined here.

In the infinitely thin model, the CFRP sheet is a flat 377-Ω surface 7.5 mm as shown in Fig. 5. Since a surface-impedance representation is taken for the CFRP sheet in FEKO, its thickness t does not need to be defined and assumed to be zero. In other words, the infinitely thin model represents salt water absorption in a Salisbury screen. While the infinitely-thin resistive sheet model is not perfectly representative of our CFRP CAA samples, analyzing this design may grant some valuable insight into salt water absorption behavior. In the finite thickness model, the CFRP sheet is given 2D-anisotropic relative permittivity data. The thickness of the CFRP sheet, t, is given the initial measured thickness of that sample. The material is given two sets of frequency-dependent relative permittivity data, representing the material in the fiber direction and orthogonal to the fiber direction. The real and imaginary values of the relative permittivity of the material in the fiber direction are $\varepsilon_r' = 1$ and $\varepsilon_r'' = \frac{\sigma}{\omega\varepsilon_0}$, respectively. Measured values of σ ranged from 10000 to 60000 S in [23]. A value of $\sigma = 10000$ S performed the best in full-wave model simulations [24]. The material in the orthogonal direction is given the initial measured permittivity data of that sample at 90°.

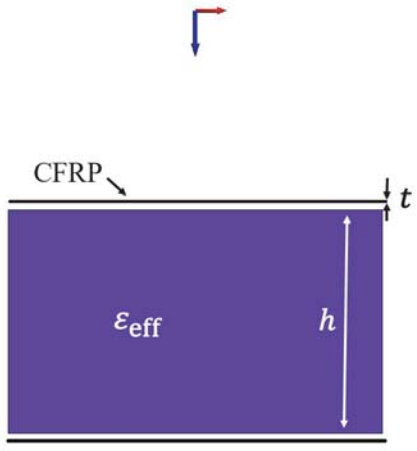

Figure 5. FEKO geometry for moisture contamination analysis. Arrows indicate direction and polarization of incident plane wave.

These samples reach maximum absorption performance at approximately 90°, and thus all simulation and measured data are shown at 90°. FEKO requests material data be inserted into the model as one of many possible choices. All of the materials used in this paper are assumed to be non-magnetic. The dielectric modeling is defined as frequency list (linear interpolation). The material is defined at specific frequencies by its relative permittivity and either its loss tangent or conductivity. The loss

tangent was calculated for all cases and imported into the model. Linear interpolation is used by FEKO in case the material is not explicitly defined at all frequencies in the solution space. For this paper, the material data are decimated to 400 frequencies across the measured range of 4 to 18 GHz to maintain accuracy without harming computational performance. Software performance was noticeably affected when material properties were defined at more that 400 frequencies. 2D-periodic boundary conditions are initialized at the boundary of the model, such that the model is effectively infinite in size. The 2D-boundary conditions are hidden from the model in Fig. 4 to clearly show the geometric features. The boundary conditions greatly ease the computational resources required to solve the problem. In FEKO, the periodic boundary condition is actually required to unlock transmission and reflection calculations. The model is excited by a linearly-polarized plane wave. Reflection coefficient data are desired at multiple angles with respect to fiber direction. The angle of polarization of the incident wave's electric field determines the reflection coefficient angle for the simulation result. Requested quantities include only the transmission and reflection coefficients whose phase plane is equi-planar with the CFRP square. Due to the ground plane being infinite in size and PEC, the transmission coefficient for this geometry will be effectively zero. The reflection coefficient solved in the simulation, then, closely represents absorption profiles for each absorber. The frequency range of interest throughout this work is 4 to 18 GHz, with a special interest at X-band frequencies.

Moisture contamination using 3.5% salinity, a representative value for sea water, is then applied to the spacer material. Pure water within a closed-cell structure, akin to that of the foam spacer, varies between its bound and unbound states and has a relative permittivity somewhere between 3.2 (similar to ice) and 80 [19]. Similarly, the relative permittivity of salt water and saline ice (frozen brine) is a function of frequency, temperature, structure, and is complex [25]. Using values from [26] as a baseline, and assuming a temperature of -5°C, the real and imaginary components of the relative permittivity of brine in equilibrium are calculated. From [26], it is evident the relative permittivity of brine follows a Debye equation very closely, and the real and imaginary components of the relative permittivity are fairly linear across the frequency band of interest. Thus, three frequencies that were highlighted in [26], namely 7.5 GHz, 9 GHz, and 11.8 GHz, are also used in this paper for simulations. The frequency-dependent values used in the exemplar simulations are presented in Table 5.

Table 5. The real (ε_r') and imaginary (ε_r'') components of the relative permittivity of salt water in a closed-cell structure.

Frequency (GHz)	ε_r'	ε_r''
7.5	42.02	28.73
9.0	36.98	28.84
11.8	30.09	28.54

The relative permittivity of the spacer is increased, symbolizing an increase of 0.5% volume fraction of salt water, from 0 to 2% for two cases: Infinitely thin CFRP sheet and CFRP sheet of thickness 0.28 mm, an average value used in our experiments. Its effect on the absorption profile of an absorber is presented in Fig. 6. The complex nature of the relative permittivity of salt water causes a downward shift in the resonant frequency and a degradation in the absorption performance of the CAA in both thickness cases. The originally lossless foam layer is now a lossy effective medium. For a volume percentage of 2%, the resonant frequency is seen to decrease by approximately 2.36 GHz for the infinitely thin case and by approximately 0.63 GHz for the finite thickness case. Furthermore, the maximum absorption level decreased by 22.93 dB in the infinitely thin model and 0.02 dB in the finite thickness model. The finite thickness model is more resilient to changes in its resonant frequency and absorption performance likely because there is already a complex term in the dielectric property of the finite thickness CFRP. Fig. 7 shows a plot of the resonant frequency downward shift as a function of volume fraction of salt water. The resonant frequency shift is referenced to the resonant frequency of the model at 0% volume fraction of salt water. Fig. 7 is used to estimate the volume percentage of brine located within the foam layer. This step requires use of measured absorption data, and thus will be discussed in Section 4.

Finally, the third model allows the thickness of the CFRP layer to vary. As the CAA absorbs

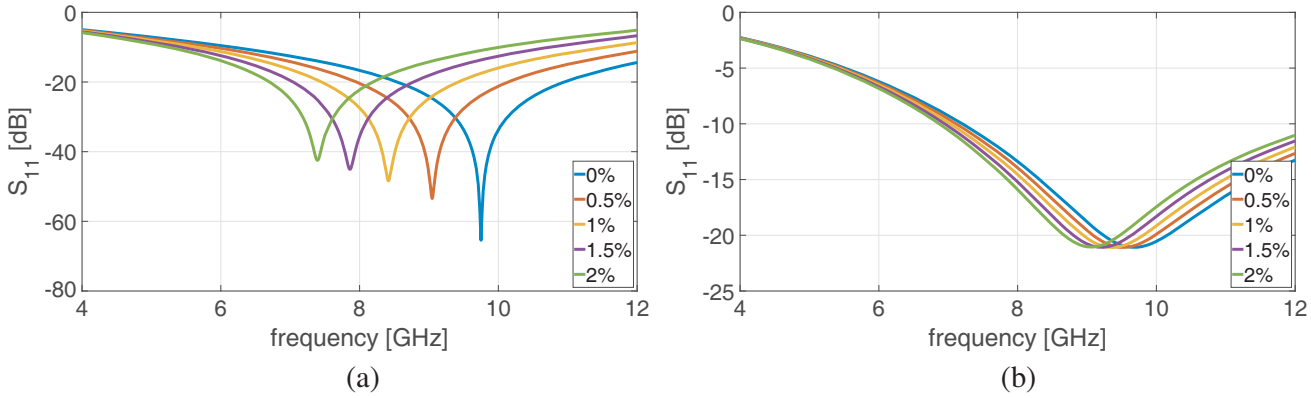

Figure 6. The effect of 3.5% saline moisture contamination on the absorption profile of an exemplar radar absorbing sandwich structure for different volume fractions and CFRP CAA models. (a) Infinitely-thin resistive sheet. (b) 0.28-mm thick impedance sheet.

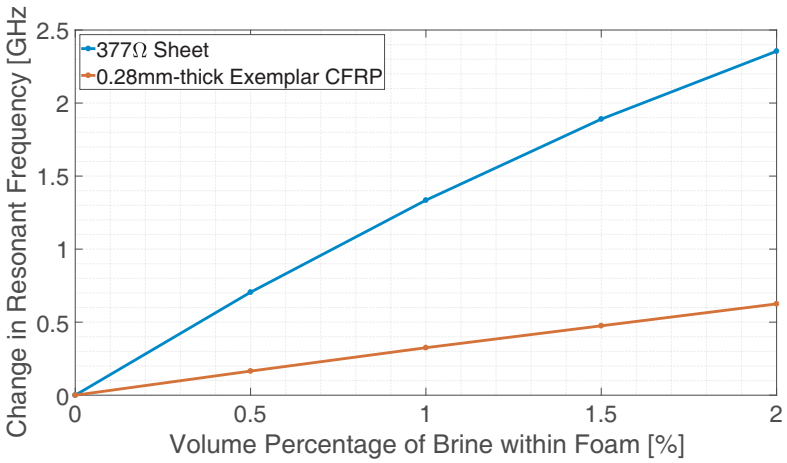

Figure 7. Downward shift in resonant frequency as a function of volume fraction of salt water for the first two CFRP models.

moisture, the CFRP layer and the foam layer are both affected and change. According to [27], composite materials infused with epoxy do absorb moisture and swell as a result. Epoxy itself is resistant to moisture, but water can penetrate through pores in the composite layer. Any water absorbed by the CFRP composite will locate voids within the matrix and fill those spaces. Voids are often found along individual fibers [28]. Thus moisture will tend to wrap around fibers and lead to matrix-weakening and swelling. Both matrix-weakening and swelling were observed in the salt water-exposed absorbers. In the third model, moisture absorption in the CFRP layer is simulated as simply an increase in the layer thickness. Any change in the dielectric properties of the CFRP layer is captured in measured data imported to the model. An initial estimate of a 10% increase for the CFRP layer thickness, values commonly seen in other works, was used [27, 28]. The percentage thickness increase is allowed, if needed, to increase slightly further due to our increased moisture exposure times, larger samples, and the inherent drawbacks of the wet-layup technique. The finite thickness model is most representative of our samples in both physical structure and electromagnetic and mechanical behavior. Thus, any further modeling will take the form of a finite thickness, anisotropic dielectric model whose CFRP layer and foam layer is subject to change.

4. MEASURED DATA

Measured data recorded throughout this work are presented and discussed here. This section focuses on the absorption profile changes caused by salt water exposure to single-ply CFRP CAAs. Plots of the absorption profile detailing the effects of salt water exposure are provided in Figs. 8 and 9. Each sample is named alphabetically in the order of fabrication, where Sample A is the first sample and Sample J is the last sample fabricated. Thus, a total of ten samples are fabricated. In the following discussion, the design frequency of a sample is assumed to be the resonant frequency of the post-fabrication, pre-exposure samples. The design frequency of each sample is shown in Table 6.

Table 6. Changes to the resonant frequency and maximum absorption level of each sample. The values shown here are the absolute values. The negative sign is suppressed.

Sample	A	B	C	D	E	F	G	H	I	J
Design Frequency (GHz)	11.13	9.54	8.73	7.31	9.62	9.09	10.50	10.47	10.60	9.54
Resonant Frequency Shift (GHz)	0.60	1.11	1.15	0.93	0.86	0.54	1.06	0.13	0.39	1.83
Maximum Absorption Level Change (dB)	1.23	6.07	6.67	5.46	6.28	9.36	2.54	6.91	10.93	7.39

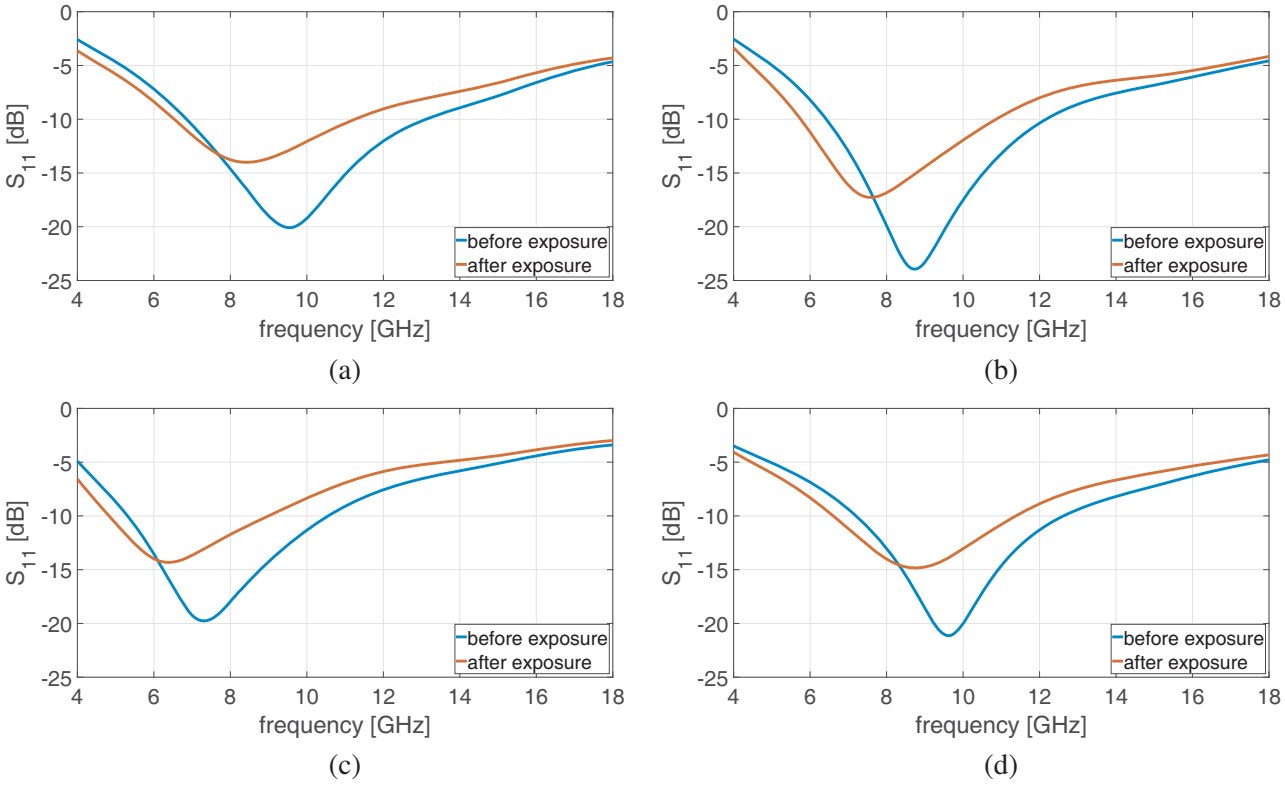

Figure 8. Comparison of pre- and post-exposure measured data for different samples. (a) Sample B. (b) Sample C. (c) Sample D. (d) Sample E.

Table 6 also displays a comparison of each sample's pre- and post-exposure states. Specifically, the table captures changes to each sample's resonant frequency and maximum absorption level. The changes are consistent in that the resonant frequency and the maximum absorption level of each of the

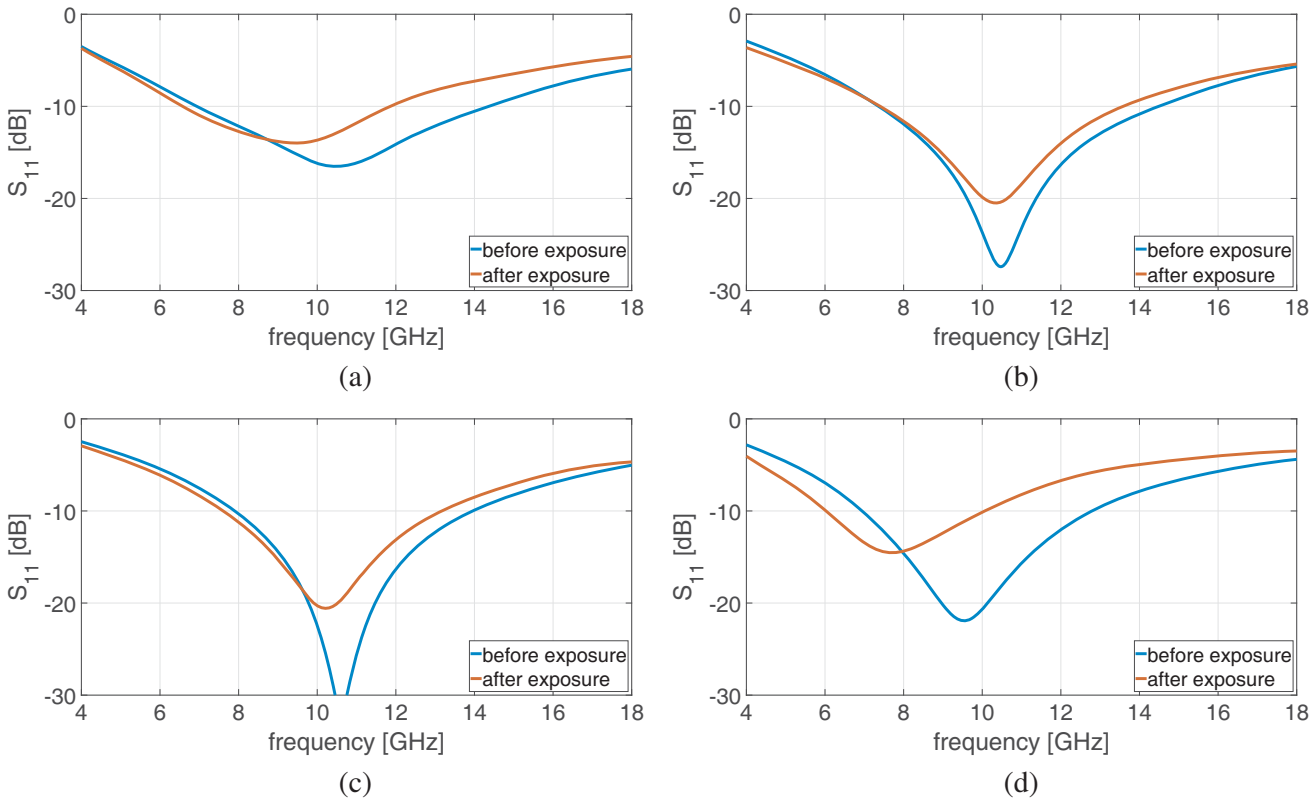

Figure 9. Comparison of pre- and post-exposure measured data for different samples. (a) Sample G. (b) Sample H. (c) Sample I. (d) Sample J.

samples decreased as deduced from Fig. 6. Every sample will be discussed in the text here; however plots for samples A and F are omitted for brevity. They both follow the same trends observed in the other samples. Samples A, B, and C, which were exposed for 10 days each, experienced an average resonant frequency shift of 0.95 GHz. Samples D, E, and F, which were exposed for 20 days each, experienced an average shift of 0.78 GHz. Finally Samples G-J were exposed for 30 days each and experienced an average resonant frequency shift of 0.85 GHz. No definitive statement can be made here regarding the differences between the duration of exposure times, except that it is very likely that the samples reach full saturation at some point before 10 days. It is clear from Refs. [7, 16, 17] that the saturation time for samples varies greatly depending on design and materials used. Since the spacer material and CFRP layer could be assumed to be fully saturated with saline water on or prior to the 10th day, we calculated the mean and standard deviation of the frequency shift using data from all ten samples A–J. These values were computed as 0.86 GHz and 0.45 GHz, respectively. In addition, the mean $\pm$ standard deviation were computed as 1.31 GHz and 0.41 GHz, respectively. These values will be used in the full-wave model.

The shift in maximum absorption level is different, however. Sample A experienced a very small change in the maximum absorption level of 1.23 dB. Meanwhile samples F and I experience a massive absorption performance degradation of 9.36 and 10.93 dB, respectively. Analyzing the average degradation for each set of samples presents a different story. The average decrease in maximum absorption level for the first set of samples is 4.66 dB, while the second and third sets experience an average of 7.04 dB and 6.94 dB, respectively. There is clearly inherent randomness here in both the physical and mechanical properties of the samples. This randomness likely propagates through to water absorption characteristics and effects for each sample. The average decrease in absorption level for all ten samples is 6.28 dB. This decrease in absorption could be catastrophic in tactical situations.

The measured weights of the samples immediately after pull from the salt water chamber and

Table 7. Changes to the weight of each sample as a result of moisture absorption.

Sample	A	B	C	D	E	F	G	H	I	J
Total Weight (g)	361.8	333.6	339.7	362.2	359.8	353.1	347.3	347.2	348.7	345.3
Δ Weight (g)	6	6.7	8	12.9	12.9	9.5	13	7.9	11	7.4

electromagnetic characterization are presented in Table 7. Table 7 also presents the Δ weight of each sample, which represents the total weight of salt water within the sample. Again, the average moisture intake for the 20-day exposure set and 30-day exposure set are higher than the 10-day set. This may indicate the saturation occurred sometime on or slightly after 10 days.

The change rate and RMSE metrics are calculated for salt water exposure on CFRP CAAs and are presented in Table 8. Whereas impact damage had wide variations of change in both resonant frequency and maximum absorption values [12], salt water exposure seems to be more consistent. This is clearly represented in the change rate and RMSE values. All of the change rates values are positive here, which shows that salt water exposure reduced the absorption performance of all of the absorbers. The average change rate, cr_A, for each set of samples is 2.54, 2.21, and 1.56, respectively. The average root-mean-square-error, RMSE_A, for each set of samples is 5.05, 4.98, and 6.19, respectively. Similar RMSE_A values signify that the total trend of the effect of salt water exposure on the absorption profile is consistent.

Table 8. Comparison of change rate, cr_A, and root-mean-square-error, RMSE_A, metrics for salt water exposure on CFRP CAAs.

Sample	cr_A (%)	RMSE_A (unitless)
A	3.11	11.63
B	3.02	3.67
C	1.48	2.83
D	2.67	6.62
E	2.52	3.77
F	1.42	5.06
G	1.81	6.11
H	0.71	5.86
I	0.80	5.32
J	2.90	3.98

Both the change rate and RMSE metrics are referenced back to the scattering parameters in a linear scale. As such, both metrics are subject to influence from the initial state performance. For example, a 6-dB change in a poorly performing initial state absorber will produce much larger cr_A and RMSE_A values than in a remarkably performing initial state absorber. This can be seen in Table 8, where the first set of samples, Samples A–C, have a higher average cr_A than the other two sets. This can be further seen in that Sample I experiences almost an 11 dB reduction in absorption performance, but the cr_A is only 0.8%.

4.1. Measured vs Modeled Results

In this section, full-wave simulation results are compared to measured results. The full-wave model simulations use measured permittivity and thickness for each respective sample, where the permittivity is measured using the free space measurement system. The thickness of each sample is measured at several points around the circumference of the sample and an average thickness is calculated. The thickness is then assumed to be equal to this average value everywhere for simulation purposes. It is important to note here that the full-wave models adhere to the same assumptions discussed above.

All salt water absorption that occurs in the CAA occurs in both the foam layer and CFRP layer. Salt water absorption manifests as a volume percentage increase of brine with respect to foam and an increase in thickness in the CFRP layer. The models in this section all use a finite thickness, 2D-anisotropic dielectric CFRP layer. Measured values of the CFRP thickness, t, the CAA height, h, and CFRP complex relative permittivity are all inputs to the model. Samples B (10-day), D (20-day), and H (30-day) are chosen to be representative samples for each sample set. The measured CAA heights (foam thickness) for the three samples presented here, B, D, and H are 3.45 mm, 4.7 mm, and 3.2 mm, respectively. The complex relative permittivity input to the model is of the form

$$\varepsilon_r(\omega) = \varepsilon_r'(\omega)\left(1 - j\frac{\varepsilon_r''(\omega)}{\varepsilon_r'(\omega)}\right) = \varepsilon_r'(\omega)\left(1 - j\tan\delta\right) \tag{1}$$

and the initial measured values for these are shown in Fig. 10. Fig. 10 also shows the initial state differences among like samples of CFRP CAAs. Each curve represents the real and imaginary components of the relative permittivity of that CFRP sample and is measured at the angle of maximum absorption, or 90 degrees.

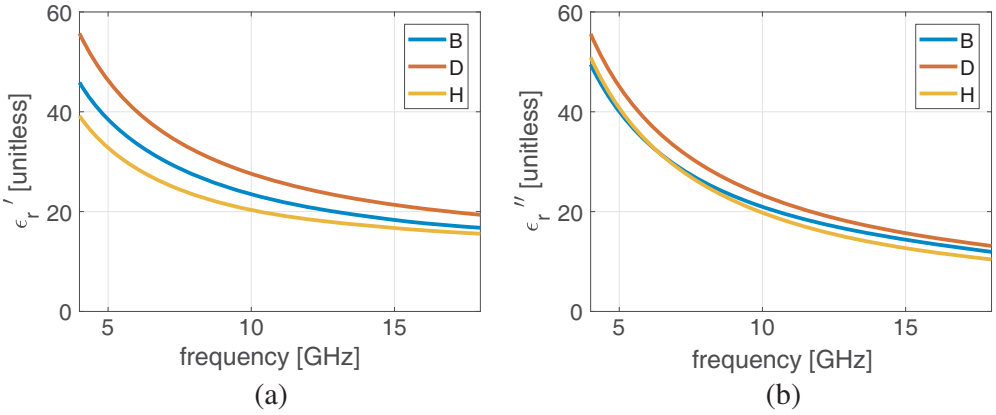

Figure 10. The (a) real and (b) imaginary components of the relative permittivity of the three samples presented in this section.

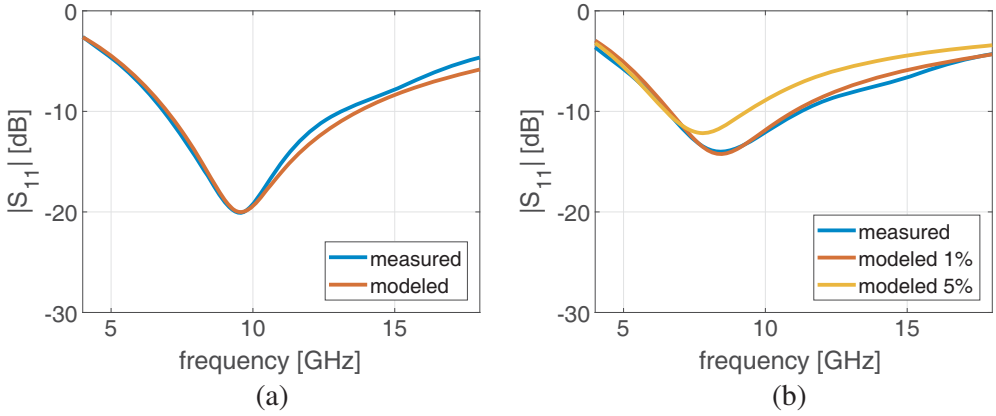

Figure 11. Comparison of pre- and post-exposure measured and modeled data for sample B. (a) Pre-exposure. (b) Post-exposure.

Figures 11–13 show the measured and modeled traces for one sample from each set of samples. The left plot in each figure compares the model results at 0% brine absorption. There is very good agreement here between the measured and modeled results at 0% brine absorption. This is understandable because there have not been any physical changes in the model due to brine absorption and the foam layer is still

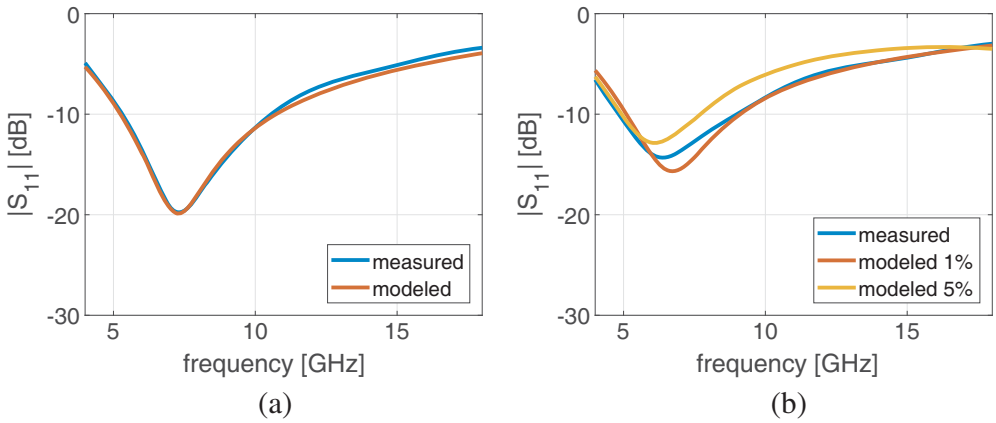

Figure 12. Comparison of pre- and post-exposure measured and modeled data for sample D. (a) Pre-exposure. (b) Post-exposure.

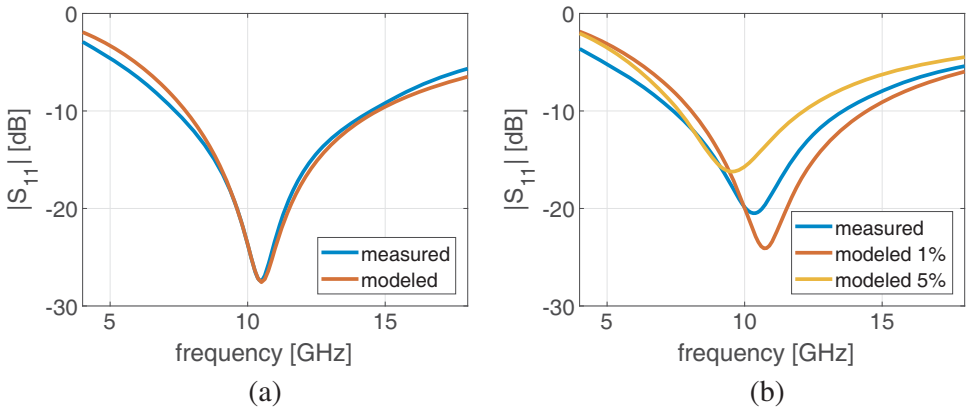

Figure 13. Comparison of pre- and post-exposure measured and modeled data for sample H. (a) Pre-exposure. (b) Post-exposure.

a lossless medium. The right plots in Figs. 11–13 compare the measured and modeled results at some finite amount of brine absorption. Since the exact volume percentage of salt water in the foam layer is unknown, we use Fig. 7 and the mean ± standard deviation frequency shift values found above as references to infer a range of possible volume percentages to guide the modeling effort. The calculated volume percentage required to cause a 1.31 GHz and a 0.41 GHz resonant frequency shift are found to be 5.12% and 1.28%, respectively, for a CFRP thickness value of 0.28 mm. These volume percentages are used as inputs in the model for each sample. Furthermore, a thickness increase is applied to each of the CFRP layers. An initial estimate of 10% is applied, but then increased slightly further for the reasons mentioned prior. The final thicknesses imported into the models are 0.33 mm for Sample B, 0.31 mm for Sample D, and 0.26 mm for Sample H. The initial thicknesses are 0.280 mm, 0.284 mm, and 0.226 mm, respectively.

The resulting absorption profiles are shown in the right plots of Figs. 11–13. In these plots, the measured data and the modeled data for both 5.12% as well as 1.28% salt water volume percentages are shown. The legends of each plot simply refer to the curves as 1% and 5%. These represent 1.28% and 5.12% salt water volume percentage, respectively. Increasing the volume percentage of brine has a similar effect as was seen prior. There is a downward shift in the resonant frequency and a degradation in the absorption performance with increasing brine absorption. The added loss mechanisms of the brine within the foam structure greatly affects the absorption profile of each absorber.

The modeled resonant frequency and absorption performance are seen to generally equate to the

measured data. The measured curves of the post-exposure samples consistently fall within the 1.28%–5.12% region. We can use these plots to estimate a more accurate percentage moisture absorption within each of the samples. From Fig. 11, it seems as though 1.28% brine absorption is an accurate estimate. From Figs. 12 and 13, Samples D and H seems to absorb more brine. A more accurate estimate for these samples could be 2% and 3%, respectively. Again, Samples D and H were left in the chamber for 10 and 20 days more than Sample B, respectively. During that time, the two samples could have absorbed more salt water. Material parameters used for the full-wave models and comparisons of the measured and modeled results are presented in Tables 9 and 10. The modeled resonant frequency and modeled maximum absorption values for each post-exposure sample are shown as a range of values from 5.12%–1.28% brine volume percentage.

Table 9. The CFRP thickness (t), measured resonant frequency ($f_{0,\text{meas}}$), and modeled resonant frequency ($f_{0,\text{mod}}$) for Samples B, D, and H before and after exposure.

Sample	t (mm)	$f_{0,\text{meas}}$ (GHz)	$f_{0,\text{mod}}$ (GHz)
B (pre)	0.280	9.540	9.63
B (post)	0.330	8.420	7.8–8.4
D (pre)	0.284	7.310	7.25
D (post)	0.310	6.380	6.1–6.7
H (pre)	0.226	10.47	10.50
H (post)	0.260	10.34	9.6–10.7

Table 10. The measured and modeled maximum absorption level for Samples B, D, and H before and after exposure.

Sample	Measured Max Absorption (dB)	Modeled Max Absorption (dB)
B (pre)	20.08	20.01
B (post)	14.01	12.16–14.24
D (pre)	19.78	19.88
D (post)	14.32	12.86–15.67
H (pre)	27.41	27.57
H (post)	20.50	16.21–24.09

There may be errors in the full-wave simulation results due to a few assumptions being taken regarding the geometry. Any physical change due to rippling or salt crystal formation on the CFRP layer is ignored in this model. The measured CFRP relative permittivity seemed to successfully capture any electromagnetic change to the CFRP. The CFRP thickness changes due to salt water absorption is also an estimated value. The CFRP thickness could not be accurately measured due to the rippling of the CFRP sheet. It is clear from this model that salt water absorption does occur within both the foam layer and CFRP layer. It is likely that the inclusion of some of the physical changes discussed above could increase the accuracy of the model. More measurement tools and apparatuses may be required to investigate this aspect in more detail. Nevertheless, our initial first order approach yields very satisfactory agreement between modeled and measured values.

Analyzing these results leads to some interesting findings. Salt water absorption certainly occurs within both the foam layer and the CFRP layer, which is supported by both the modeled and measured data and other work. Changing the fabrication method of the CFRP CAA from a wet-layup technique to a pre-preg technique could reduce salt water penetration and absorption. Changes to the design could also be explored, albeit being careful not to change the electromagnetic properties of the absorbing

structure. Based on the results presented in this paper, it may be concluded that exposure to salt water critically limits and hinders the performance of CFRP CAAs. In our prior work, impact damage was also shown to negatively affect the performance of CFRP CAAs [12]. The main difference, however, is that it seems that salt water exposure has a more consistent and predictable effect on CFRP CAAs than uncontrolled impact damage. We can state definitively that salt water exposure will lead to a decrease in the absorption profile and a decrease in the resonant frequency of CFRP CAAs. While this statement is true, the effects of each factor should be discussed and considered. The primary contributor of the resonant frequency downward shift is the increase in the relative permittivity of the spacer material and increase in the spacer thickness. Both of these can be attributed to salt water penetrating the foam layer. The primary contributor to the decrease in the absorption profile is the lossy component added to the spacer material and the change in the relative permittivity of the CFRP layer. Both of these, as well, are attributed to salt water penetrating the layers. Salt crystal formation on the CFRP layer also influences the CFRP layer's relative permittivity, but to an unknown degree. From this discussion, it seems that if this experiment were to be repeated, but using pure water instead of salt water, the downward trend in the resonant frequency would be similar, but the absorption profile may not decrease as much. Such a study would be a great candidate for future work.

5. CONCLUSIONS

This paper has explored changes to the absorption profile of an electromagnetic absorber under potential environmental conditions. Specifically, changes to the absorption level across a frequency band of interest due to salt water fog exposure is measured and modeled. A salt water fog chamber was implemented to subject the samples to controlled fog exposure. Multiple instrumentation values were monitored and controlled throughout the exposure process. Free space characterization data was captured using a VNA for use in a full-wave simulation model. A Method of Moments, frequency-domain solver was used for all simulations. The full-wave model agreed strongly with the measured data, giving confidence that the model is accurate. The methods presented here can potentially be adapted and applied to other materials or absorber configurations. Salt fog exposure has been shown to degrade the electromagnetic performance of a unidirectional CFRP CAA. Rippling in the CFRP, salt crystal formation, and swelling have been identified as physical changes that occur to a CFRP CAA in salt water exposure. A decrease in both the resonant frequency and maximum absorption level has been identified as electromagnetic changes that CFRP CAAs experience due to salt water exposure.

Future work will investigate other sources of damage or degradation. There are many other environmental conditions, such as cyclic loading, temperature changes, sand particle impacts, and UV radiation that can severely degrade a composite material and its electromagnetic behavior. Each of these can and should be studied to further characterize these degradation effects. Other designs and materials should also be studied. What was researched here, unidirectional CFRP with a closed-cell vinyl foam, is just one of many possible configurations for composite RAM.

ACKNOWLEDGMENT

This work was supported through a Pennsylvania State University Applied Research Laboratory (ARL) Graduate Walker Assistantship. We appreciate the assistance provided by T. J. Eden of ARL during sample preparation.

REFERENCES

1. Mangalgiri, P. D., "Composite materials for aerospace applications," *Bull. Mater. Sci.*, Vol. 22, No. 3, 657–664, 1999.
2. Mouritz, A. P., E. Gellert, P. Burchill, and K. Challis, "Review of advanced composite structures for naval ships and submarines," *Compos. Struct.*, Vol. 53, No. 1, 21–22, 2001.
3. Shen, C. H. and G. S. Springer, "Moisture absorption and desorption of composite materials," *J. Compos. Mater.*, Vol. 10, No. 1, 2–20, 1976.

4. Springer, G. S., "Environmental effects on epoxy matrix composites," *Composite Materials: Testing and Design (Fifth Conference)*, 291–312, Tsai S. W. (ed), Philadelphia, PA, 1979.
5. Shirrell, C. D. and J. Halpin, "Moisture absorption and desorption in epoxy composite laminates," *Composite Materials: Testing and Design (Fourth Conference)*, 514–528, Davis Jr, J. G. (ed), Philadelphia, PA, 1977.
6. Selzer, R. and K. Friedrich, "Mechanical properties and failure behaviour of carbon fibre-reinforced polymer composites under the influence of moisture," *Compos. Part A*, Vol. 28, No. 6, 595–604, 1997.
7. Almudaihesh, F., K. Holford, R. Pullin, and M. Eaton, "The influence of water absorption on unidirectional and 2D woven CFRP composites and their mechanical performance," *Compos. Part B*, Vol. 182, 107626, 2020.
8. Jafar, H. I., S. I. Husaen, and E. A. Al-Ajaj, "Effect of water absorption on some electrical and dielectrical properties of epoxy resin reinforced with chopped carbon fibers," *Al-Nahrain J. Sci.*, Vol. 14, 87–94, 2011.
9. Gadja, W. J., "Measurement of the electrical properties of composite materials in the frequency range of DC to 30 MHz," Report RADC-TR-79-03, Syracuse University, USA, August 1979.
10. Munk, B., *Frequency Selective Surfaces: Theory and Design*, Wiley, New York, NY, USA, 2000.
11. Fante, R. L. and M. T. McCormack, "Reflection properties of the Salisbury screen," *IEEE Trans. Antennas Propag.*, Vol. 36, No. 10, 1443–1454, 1988.
12. O'Donnell, J. C. and R. M. Narayanan, "Impact damage characterization for varying areal-weight unidirectional carbon fiber-reinforced polymer circuit-analog absorbers," *Compos. Part B*, Vol. 202, 108427, 2020.
13. O'Donnell, J. C., R. M. Narayanan, and E. H. Lenzing, "Analysis of damage in unidirectional CFRP circuit analog absorbers," *IEEE National Aerospace and Electronics Conference (NAECON 2018)*, 555–560, Dayton, OH, USA, IEEE, Piscataway, July 23–26, 2018.
14. O'Donnell, J. C., E. J. Riley, and R. M. Narayanan, "Electromagnetic response changes of unidirectional carbon fiber-reinforced polymer circuit-analog absorbers due to post-processing impact damage," *SPIE Conference on Radar Sensor Technology XXIII*, Baltimore, MD, USA, SPIE, Bellingham, WA, April 14–18, 2019.
15. Riley, E. J., E. H. Lenzing, and R. M. Narayanan, "Application of unidirectional carbon-fiber-reinforced-polymer laminas in circuit-analog absorbers," *IEEE Trans. Electromagn. Compat.*, Vol. 60, No. 6, 1743–1751, 2018.
16. Zafar, A., F. Bertocco, J. Schjødt-Thomsen, and J. C. Rauhe, "Investigation of the long term effects of moisture on carbon fibre and epoxy matrix composites," *Compos. Sci. and Tech.*, Vol. 72, No. 6, 656–666, 2012.
17. Gao, C. and C. Zhou, "Moisture absorption and cyclic absorption-desorption characters of fibre-reinforced epoxy composites," *J. Mater. Sci.*, Vol. 54, 8289–8301, 2019.
18. Kafodya, I., G. Xian, and H. Li, "Durability study of pultruded CFRP plates immersed in water and seawater under sustained bending: Water uptake and effects on the mechanical properties," *Compos. Part B*, Vol. 70, 138–148, 2015.
19. Grace, L. R., "The effect of moisture contamination on the relative permittivity of polymeric composite radar-protecting structures at X-band," *Compos. Struc.*, Vol. 128, 305–312, 2015.
20. Fink, B. K., R. L. McCullough, and J. W. Gillespie, "The influence of moisture on dielectric behavior of poly-etheretherketone/carbon fiber composites," *J. Thermoplast. Compos. Mater.*, Vol. 5, No. 2, 90–104, 1992.
21. Reid, J. D., W. H. Lawrence, and R. P. Buck, "Dielectric properties of an epoxy resin and its composite I. Moisture effects on dipole relaxation," *J. Appl. Polym. Sci.*, Vol. 31, 1771–1784, 1986.
22. Diab Group, Divinycell H datasheet, www.diabgroup.com/en-GB/Products-and-services/Core-Material/Divinycell-H (2020, accessed 5 March 2020).
23. Im, K.-H., et al., "Influence of terahertz waves on unidirectional carbon fibers in CFRP composite materials," *Mater. Sci. (Medžiagotyra)*, Vol. 20, No. 4, 457–463, 2014.

24. Riley, E. J., E. H. Lenzing, and R. M. Narayanan, "X-band circuit-analog absorbers using unidirectional carbon-fiber laminas," *IEEE Antennas Wirel. Propag. Lett.*, Vol. 17, No. 6, 1060–1063, 2018.
25. Morey, R. M., A. Kovacs, and G. F. N. Cox, "Electromagnetic properties of sea ice," *Cold Regions Science and Technology*, Vol. 9, No. 1, 53–75, 1984.
26. Stogryn, A. and G. J. Desargant, "The dielectric properties of brine in sea ice at microwave frequencies," *IEEE Trans. Antenna and Propag.*, Vol. 33, No. 5, 523–532, 1985.
27. Khalil, H. P. S. A., M. Jawaid, and A. A. Bakar, "Woven hybrid composites: Water absorption and swelling behaviours," *BioResour.*, Vol. 6, No. 2, 1043–1052, 2011.
28. Mariatti, M., M. Jannah, A. A. Bakar, and H. P. S. A. Khalil, "Properties of banana and pandanus woven fabric reinforced unsaturated polyester composites," *J. Compos. Mater.*, Vol. 42, No. 9, 931–941, 2008.